Chaos, Solitons and Fractals 187 (2024) 115421

Contents lists available at ScienceDirect

Chaos, Solitons and Fractals

journal homepage: www.elsevier.com/locate/chaos

Lévy noise-induced effects in a long Josephson junction in the presence of two different spatial noise distributions

Claudio Guarcello [a,b], Giovanni Filatrella [c,b], Duilio De Santis [d,*], Bernardo Spagnolo [d,e], Davide Valenti [d]

[a] Dipartimento di Fisica "E.R. Caianiello", Università di Salerno, Via Giovanni Paolo II, 132, I-84084 Fisciano (SA), Italy
[b] INFN, Sezione di Napoli Gruppo Collegato di Salerno, Complesso Universitario di Monte S. Angelo, I-80126 Napoli, Italy
[c] Department of Sciences and Technologies and Salerno unit of CNISM, University of Sannio, Via Port'Arsa 11, Benevento I-82100, Italy
[d] Dipartimento di Fisica e Chimica "Emilio Segrè", Group of Interdisciplinary Theoretical Physics, Università degli Studi di Palermo, Viale delle Scienze, Edificio 18, I-90128 Palermo, Italy
[e] Stochastic Multistable Systems Laboratory, Lobachevsky University, 603950 Nizhniy Novgorod, Russia

ARTICLE INFO

Keywords:
Lévy noise
Long Josephson junctions
Average switching time
Nonequilibrium statistical mechanics

ABSTRACT

We analyze the impact of Lévy-distributed stochastic fluctuations on the average switching time and voltage drop across a current-biased long Josephson tunnel junction. We compare the system's response for two spatial configurations of time-dependent noise, *i.e.*, homogeneous and distributed along the junction length. The response of the Josephson junction is explored by varying the characteristic parameter of the Lévy source, *i.e.*, the α stability index and the noise intensity. These findings offer an effective tool to characterize a Lévy component possibly embedded in an unknown noise signal.

1. Introduction

Solitonic excitations, characterized by their localized and robust nature, have captivated the interest of researchers across various scientific disciplines [1]. In the realm of solid state physics, long Josephson junctions (LJJs) emerge as a remarkable platform for the study of solitons, particularly kinks and breathers [2–6]. The term "long" refers to a mesoscopic device consisting of a thin insulating layer sandwiched between two superconducting electrodes with one dimension on the order of several Josephson penetration depths, *i.e.*, the typical length scale of the system [7]. This aspect promotes the emergence of various solitonic phenomena [2–6]. Substantial experimental progresses have enabled the direct observation and manipulation of solitonic excitations in LJJs, and theoretical efforts supported by numerical simulations have played a crucial role in elucidating the dynamics and stability of these nonlinear modes [5,8].

Solitonic excitations in LJJs are not immune to the influence of external random perturbations, *i.e.*, noise. The latter, arising from various sources such as thermal fluctuations and imperfections in the system, introduces stochastic effects, which can significantly affect the dynamics and stability of solitons. We note that random fluctuations are always present in open systems, such as, for instance, biological and ecological systems [9,10] and financial markets [11], and cannot be therefore neglected in a faithful description of their dynamics. In particular, understanding the interplay between Josephson dynamics and noise is crucial for comprehending, e.g., the solitons' behavior in realistic environments and designing robust applications [12–20]. Thus, noise-induced effects on Josephson devices represent a fertile theoretical research topic in both short and long junction cases [21–30].

In this work, we examine the role of noise in LJJs, considering the joint effect of two time-dependent noise contributions, *i.e.*, Gaussian and Lévy. Regarding Lévy noise, we compare two distinct cases: a spatially distributed delta-correlated source and a spatially homogeneous source. In a realistic device, *i.e.*, an LJJ, the two types of noise sources can have different physical origins: in the homogeneous case, from fluctuations in the current generator, while in the distributed case, from the array of independent small junctions connected in parallel to form the LJJ.

The response of the device is found to be profoundly different for the two types of fluctuations, inasmuch solitons are only formed in the case of distributed sources. Conversely, in the case of a homogeneous source, the overall switching dynamics consists of the entire "phase string" overcoming the potential barrier that confines the system into the superconducting state.

The fact that the two types of noise distributions differently affect the switching dynamics is directly reflected in the behavior of both the average lifetime of the superconducting state and the average voltage

* Corresponding author.
E-mail addresses: cguarcello@unisa.it (C. Guarcello), duilio.desantis@unipa.it (D. De Santis).

https://doi.org/10.1016/j.chaos.2024.115421
Received 14 July 2024; Received in revised form 17 August 2024; Accepted 19 August 2024

drop. The former quantity concerns the transition from the superconductive to the voltage state, while the latter describes the dynamical regime established once a switching has occurred. Both responses are of great practical relevance, as these two quantities can be experimentally measured.

The paper is organized as follows. In Section 2 we present the theoretical groundwork for the time evolution of the Josephson phase in an LJJ, the statistical properties of the Lévy noise, and the method to face the stochastic simulations. In Section 3, the results are discussed and analyzed: in particular, we compare the noise-intensity dependence of both the average switching time and the average voltage drop in the case of a spatially distributed (see Section 3.1) and homogeneous (Section 3.2) Lévy noise source. We also investigate in Section 3.3 the responsivity of the device in these two cases and, finally, in Section 3.4 we look at the effects of the temperature at which the junction operates. In Section 4, conclusions are drawn.

2. The theoretical framework

A Josephson tunnel junction is formed by sandwiching a thin insulating layer between two superconducting electrodes. In the long junction limit, one of the lateral dimensions, $\mathcal{L}$ and $\mathcal{W}$, is greater than the Josephson penetration depth, namely, $\mathcal{L} > \lambda_J$ and $\mathcal{W} \ll \lambda_J$, with $\lambda_J = \sqrt{\frac{\Phi_0}{2\pi\mu_0}\frac{1}{t_d J_c}}$ being the Josephson penetration length [7]. Here, $t_d = \lambda_{L,1} + \lambda_{L,2} + d$ is the effective magnetic thickness (with $\lambda_{L,i}$ and d being the London penetration depth of the i-the electrodes and the insulating layer thickness, respectively), μ_0 is the vacuum magnetic permeability, and J_c is the critical current area density.

The setup considered in this work consists of an LJJ traversed by two superimposed electric currents, that is I_b and I_N, a known bias current drawn from a parallel source and a stochastic noise current, respectively. The injected bias current, which is essential for characterizing the stochastic component, is set below the critical value to maintain the system in the superconductive metastable state. This allows the noise to eventually push the system out of this state, inducing a switch from the zero-voltage state to the finite-voltage "running" state. The running state results in a detectable non-zero voltage drop, according to the a.c. Josephson relation $V = (\Phi_0/2\pi)d\varphi/dt$ [31,32], where φ is the phase difference between the wave functions of the superconducting condensates in the two electrodes and $\Phi_0 = h/2e \simeq 2 \times 10^{-15}$ Vs is the magnetic flux quantum. The escape mechanisms driven by macroscopic quantum tunneling [33] can be neglected if the working temperature is above the crossover value, that is, at temperatures at which thermal escapes dominate.

The response of an LJJ can be described in terms of a partial differential equation, *i.e.*, the perturbed sine-Gordon (SG) equation, for the phase φ. In normalized units it can be written as [7,34]

$$\beta_C \frac{\partial^2\varphi(x,t)}{\partial t^2} + \frac{\partial\varphi(x,t)}{\partial t} - \frac{\partial^2\varphi(x,t)}{\partial x^2} + \sin[\varphi(x,t)] = i_N(x,t) + i_b. \tag{1}$$

The boundary conditions include the external magnetic field H_{ext}

$$\frac{\partial\varphi(0,t)}{\partial x} = \frac{\partial\varphi(L,t)}{\partial x} = 2\frac{H_{\text{ext}}(t)}{H_{c,1}}, \tag{2}$$

where $H_{c,1} = \frac{\Phi_0}{\pi\mu_0 t_d \lambda_J}$ is the so-called first critical field of the junction [35]. In this work, however, the magnetic field is set to zero, $H_{\text{ext}}(t) = 0$. In the equations, we use dimensionless space and time variables, x and t, respectively, normalized to the Josephson penetration depth λ_J, and to the inverse of the characteristic frequency $\omega_C = (2e/\hbar)I_c R$ of the junction (here, I_c is the critical current and R is the normal-state resistance of the junction). Moreover, $\beta_C = \omega_c RC$ is the Stewart-McCumber parameter. Eq. (1) consists of different parts: the Josephson elements at the left hand side, the external bias current $i_b = I_b/I_c$, and a noise source $i_N(t) = I_N(t)/I_c$. In this work, the random current is modeled as a mixture of a standard Gaussian white noise and a stochastic Lévy process, and is obtained with the approximated finite independent increments [36].

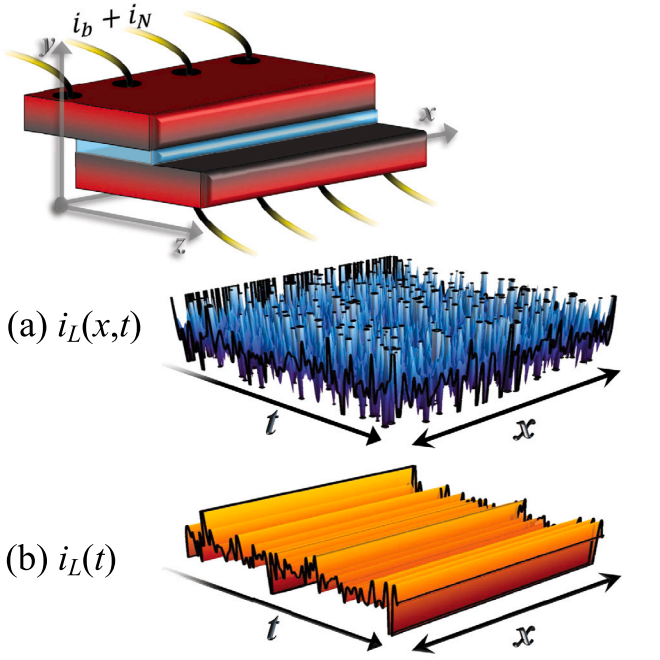

Fig. 1. Cartoon of a LJJ biased by both a constant and a noise current, i_b and i_N, respectively. The bottom panels sketch the two spatial configurations of noise current taken into account in this work: (a) many (infinite) independent, spatially distributed Lévy noise sources, $i_L(x,t)$, and (b) a homogeneous Lévy noise source, $i_L(t)$, affecting the whole system.

The SG equation supports a traveling wave solitonic solution, called *kink* [5], *i.e.*, a 2π-phase twist that corresponds to a flux quantum Φ_0 along the junction [3]. Thus, a kink is usually referred to as a *fluxon* or Josephson vortex in this context. The fluxon has a width of the order of λ_J and is surrounded by a flowing supercurrent circulating around it.

The Lévy noise statistics describes abrupt jumps and very rapid variations, called *Lévy flights*. In fact, the heavy tails that characterize the distribution of Lévy fluctuations cause the occurrence of large variations with non-negligible probability. Lévy flights are frequently used to address transport phenomena across condensed matter systems and practical applications [37–54]. For instance, the presence of Lévy fluctuations was recently discussed in graphene [55–59]. For an extensive bibliography on examples and applications, in which Lévy-distributed fluctuations can be observed, see Refs. [28,29].

We first consider spatially distributed non-Gaussian noise fluctuations, $i_N(x,t)$; in other words, we assume an array of independent delta-correlated noise sources, one for each element Δx of the junction length. In this case, the stiffness of the Josephson phase along the system can play an important role in the noise-triggered switching dynamics. In fact, although a Lévy flight can cause a phase fluctuation large enough to "push" a single portion of the junction out of the metastable superconducting state, a sufficiently large intensity is required to overcome the phase rigidity and trigger kinks, thus inducing the switching of the entire system. Otherwise, these fluctuations can induce other types of small-amplitude excitations, which rapidly decay (*e.g.*, breather-like solutions) without causing the whole system to switch. We compare the case of independent noise sources distributed along the junction with the case of a homogeneous noise source, $i_N(t)$, applied to the entire phase string. In the uniform case, as already mentioned, we expect the noise not to generate kinks.

If we consider both Gaussian and Lévy noise sources, with amplitudes γ_G and γ_L, respectively, the stochastic independent increment reads

$$\Delta i_N = \Delta i_G + \Delta i_L \simeq 2\Delta x \Delta t \left[\sqrt{2\gamma_G \Delta x \Delta t}\, N(0,1) + \left(\gamma_L \Delta x \Delta t\right)^{\frac{1}{\alpha}} S_\alpha(1,0,0) \right]. \quad (3)$$

Here, the symbol $N(0,1)$ indicates a Gaussian random variable, with zero mean and unit standard deviation, while $S_\alpha(1,0,0)$ denotes a *standard* α-stable random Lévy variable. In general, the notation $S_\alpha(\sigma,\beta,\lambda)$ is used for indicating Lévy distributions [27], where $\alpha \in (0,2]$ is the *stability index*, $\beta \in [-1,1]$ is called *asymmetry parameter*, and $\sigma > 0$ and λ are a scale and a location parameter, respectively. The stability index characterizes the asymptotic power law for the distribution, which for $\alpha < 2$ is of the $|x|^{-(1+\alpha)}$ type, while for $\alpha = 2$ is the Gaussian distribution. In fact, the probability density function of a normal distribution $N(\lambda,\sigma)$ is equivalent to that of the stable distribution $S_2(\sigma/\sqrt{2},\beta,\lambda)$. In this work, we consider exclusively symmetric (*i.e.*, with $\beta = 0$), bell-shaped, standard (*i.e.*, with $\sigma = 1$ and $\lambda = 0$), stable distributions $S_\alpha(1,0,0)$, with $\alpha \in [0.1,2]$. To model the Lévy noise sources, we use the algorithm proposed by Weron [60,61] for the implementation of the Chambers method [62]. The stochastic dynamics of the system is investigated by integrating Eq. (1) with an implicit finite-difference method based on a tridiagonal algorithm, using space and time integration steps equal to $\Delta x = \Delta t = 5 \times 10^{-2}$, and choosing $\varphi(x,0) = \arcsin(i_b)$ and $\partial\varphi(x,0)/\partial t = 0$ as initial condition.

Let us give some physical considerations on the parameter γ_G in Eq. (3). For the pure Gaussian noise case, *i.e.*, $\gamma_L = 0$ so that $I_N \equiv I_G$, the statistical properties of the current fluctuations, in normalized units, are given by

$$\begin{aligned} \mathrm{E}\left[i_G(x,t)\right] &= 0, \\ \mathrm{E}\left[i_G(x,t) i_G\left(x+\tilde{x}, t+\tilde{t}\right)\right] &= 2\gamma_G(T)\delta(\tilde{x})\,\delta(\tilde{t}), \end{aligned} \quad (4)$$

where $E[\cdot]$ is the expectation operator and the amplitude of the normalized correlator is connected to the physical temperature T through the relation [21]

$$\gamma_G(T) = \frac{k_B T}{E_{J_0}} L, \quad (5)$$

where $E_{J_0} = \left(\Phi_0/2\pi\right) I_c$. For a junction with $L = 10$, $I_c = 1$ μA, and $T = 250$ mK, the dimensionless noise intensity is $\gamma_G \sim 10^{-1}$.

In the following, we look in detail at how some key quantities, i.e., the mean switching time, the average voltage drop, and the soliton density, depend on different noise-source parameters, that is, the noise intensity and the stability index α.

The mean switching time (MST) toward the resistive state, starting from the metastable state identified by the washboard potential minimum, is computed as a nonlinear relaxation time (NLRT) [23–25]. We obtain the residence time of the phase φ within the relative maxima $\varphi^L_{\max}$ and $\varphi^R_{\max}$ to the left and the right of the minimum, i.e., $\varphi \in [\varphi^L_{\max}\ ,\ \varphi^R_{\max}]$, imposing no absorbing barriers, so that within the whole measurement time, $t_{\max}$, all possible temporary trapping events contribute to the calculation of the residence time [63–67]. In the ith numerical realization for the jth junction portion, the probability P_{ij} that $\varphi_j \in [\varphi^L_{\max}\ ,\ \varphi^R_{\max}]$ is

$$P_{ij}(t) = \begin{cases} 1 & \text{if} \quad \varphi_j \in [\varphi^L_{\max}\ ,\ \varphi^R_{\max}]. \\ 0 & \text{if} \quad \varphi_j \notin [\varphi^L_{\max}\ ,\ \varphi^R_{\max}]. \end{cases} \quad (6)$$

Summing $P_{ij}(t)$ over the total number $N_c = L/\Delta x$ (here, L is the normalized junction length) of elements and over the number N_{exp} of realizations, the average probability that the entire string is in the superconducting state at time t can be computed as

$$\overline{P}(t) = \frac{1}{N_{\mathrm{exp}}\, N_c} \sum_{i=1}^{N_{\mathrm{exp}}} \sum_{j=1}^{N_c} P_{ij}(t). \quad (7)$$

Finally, the MST $\langle\tau\rangle$ is calculated as the time spent on average in the superconducting state. According to the definition of P_{ij} of Eq. (6), this quantity is given by

$$\langle\tau\rangle = \int_0^{t_{\max}} \overline{P}(t) dt. \quad (8)$$

The upper extreme of integration, i.e., $t_{\max}$, should be infinite for the proper MST calculation [67]; obviously, in numerical calculations, this limit is chosen finite but reasonably large, so as to capture the essential dynamical aspects. The procedure is repeated varying the noise index α and intensity γ_L to retrieve the behavior of the MST in the presence of different sources of Lévy noise.

The response to the noise of an LJJ can be also analyzed through the junction average voltage or by the noise-induced kink generation rate. In this case as well, we perform a double average over ensemble and time. Thus, in the ith numerical realization, the average voltage drop (normalized to $\Phi_0\omega_C$) across the junction is given by

$$\begin{aligned} \langle V_i \rangle &= \frac{1}{2\pi} \frac{1}{t_{\max}} \frac{1}{L} \int_0^L \int_0^{t_{\max}} \frac{d\varphi_i(x,t)}{dt} dt dx \\ &= \frac{1}{2\pi} \frac{1}{t_{\max}} \left[\frac{1}{L} \int_0^L \varphi_i\left(x, t_{\max}\right) dx - \arcsin(i_b) \right], \end{aligned} \quad (9)$$

where $\varphi_i(x,0) = \arcsin(i_b)$ represents the initial phase profile. Then, the average voltage drop results from the average over the total number of independent numerical realizations, N_{exp}, that is

$$\langle V \rangle = \frac{1}{N_{\mathrm{exp}}} \sum_{i=1}^{N_{\mathrm{exp}}} \langle V_i \rangle. \quad (10)$$

The features shown by the voltage response of the device can be grasped by looking also at the number of kinks generated along the junction, which, in the ith realization, can be estimated as [68]

$$N_i(t) = \left\lfloor \frac{\varphi(L,t) - \varphi(0,t)}{2\pi} \right\rfloor, \quad (11)$$

where $\lfloor ... \rfloor$ stands for the integer part of the argument. Finally, the average kink density is obtained as

$$\langle n \rangle = \frac{1}{N_{\mathrm{exp}}} \sum_{i=1}^{N_{\mathrm{exp}}} \frac{N_i(t_{\max})}{L}. \quad (12)$$

3. Results and discussions

In this section we analyze the response of an LJJ biased by a noise current composed of many independent spatially distributed sources (see Fig. 1a), and of a homogeneous source (see Fig. 1b). In the latter condition, we stress again that the noise can only induce the uniform rolling down of the phase along the potential profile, with no kink generation.

The values of the average time $\langle\tau\rangle$ and voltage $\langle V\rangle$ are obtained by setting a measurement time equal to $t_{\max} = 10^4$ and averaging over $N_{\mathrm{exp}} \simeq 10^5$ independent numerical repetitions. Moreover, we consider an intermediate damping case, $\beta_C = 1$, a junction length equal to $L = 20$, and a bias current $i_b = 0.2$. In Sections 3.1–3.3, we neglect Gaussian thermal fluctuations (*i.e.*, we set $\gamma_G = 0$) to elucidate the role of Lévy flights on the phase dynamics, while the study of the Gaussian noise effects is postponed to Section 3.4.

3.1. Case (a): distributed noise sources

In Fig. 2(a) we show how the MST, $\langle\tau\rangle$, calculated through Eq. (8), depends on the noise intensity and the stability index α in the case of spatially delta-correlated noise sources, i.e., the case (a) in Fig. 1. Let us first look at $\alpha = 2$ (*i.e.*, the red curves), which is quite peculiar, since the Lévy distribution coincides with the Gaussian noise. We observe a plateau at $\langle\tau\rangle = t_{\max}$, which is nothing but a numerical artifact due to an insufficiently long measurement time, below a certain noise

intensity, which is marked by a black vertical long-dashed line. This threshold value, γ_L^{th}, can be roughly estimated as the noise intensity at which the measurement time matches the inverse of the escape Kramers rate [69] from a potential barrier ΔU,

$$\Gamma(i_b,\gamma)=\frac{\omega_A}{2\pi}e^{-\frac{\Delta U}{k_BT}}. \tag{13}$$

We now assume that this confinement potential barrier coincides with the activation energy for kink/antikink generation, the noise distribution being capable of inducing this type of excitation in this case; for a long enough junction, $L \gtrsim 6$, such an energy approaches the value $L\Delta U/E_{J_0} \sim 8$ [21]. In terms of the bias-tilted washboard potential barrier height, $\Delta U(i_b) = \Delta U(i_b)/E_{J_0} = 2\left[\sqrt{1-i_b^2} - i_b \arccos(i_b)\right]$, and the normalized noise intensity defined in Eq. (5), the Kramers escape rate becomes

$$\Gamma_{(a)}(i_b,\gamma)=\frac{\omega_c}{2\pi}\left(1-i_b^2\right)^{\frac{1}{4}}e^{-\frac{8\Delta U(i_b)}{\gamma}}, \tag{14}$$

assuming the attempt frequency $\omega_A=\omega_c\left(1-i_b^2\right)^{\frac{1}{4}}$ of a single JJ. Thus, the condition $t_{\max}\equiv\Gamma_{(a)}^{-1}(i_b,\gamma_L^{th}/\sqrt{2})$ [70] is satisfied by a noise intensity of $\gamma_L^{th}\sim 0.4$ (see the black dashed line in Fig. 2).

The MST curves for a genuine Lévy flight, $\alpha<2$, smoothly approach, at low noise intensities, a plateau at $\langle\tau\rangle\sim t_{\max}$, but the γ_L value at which it is reached tends to decrease with α. The matching condition between the measurement time and the inverse escape rate, used to obtain γ_L^{th} for $\alpha=2$, does not work when considering the escape rate for $\alpha<2$ (data not shown). Indeed, the power-law dependence [71,72] for $\alpha<2$, which gives rise to Lévy flights, entails also a non-vanishing probability of escape even at times shorter than $t_{\max}$; moreover, the longer the simulation time, the greater the probability of these rare events to occur. In other words, the threshold noise intensity, below which the curves for $\alpha<2$ approach a plateau, changes with $t_{\max}$ not just because of a longer measurement time, but also because the system has more time to "incur" in a Lévy flight, as observed for short JJs [29].

As the noise intensity γ_L grows, $\langle\tau\rangle$ monotonically decreases. The $\left\langle\tau\left(\gamma_L\right)\right\rangle$ curves at different α appear clearly separated and well spaced, in agreement with previous investigations of barrier crossing in metastable potential profiles [72]. For $\gamma_L\lesssim 2$, at a fixed noise intensity, a lower α corresponds always to a faster escape, *i.e.*, a smaller $\langle\tau\rangle$, because Lévy flights become more frequent. However, for $\alpha\gtrsim 1$ we note the formation of a sort of "knee" at $\langle\tau\rangle\gtrsim 50$. Looking at rather high noise intensities, $\gamma_L>2$, the MST *versus* α at a fixed γ_L shows a non-monotonic trend.

In Fig. 2(b) we illustrate the behavior of the average voltage drop $\langle V\rangle$ as a function of the Lévy noise intensity γ_L, for different values of α. One immediately notices the opposite behavior of $\langle V\rangle$ compared to MST, i.e., at a given noise intensity, the lower α, the larger is the time derivative of the phase due to Lévy flights; as a consequence, $\langle V\rangle$ increases.

Interestingly, at "low" noise intensities, *i.e.*, for $\gamma_L\lesssim\gamma_L^{th}$, the different $\langle V\rangle$ *versus* γ_L curves arrange, in a log–log scale, in well-distinct parallel lines with a positive slope. This region of γ_L values will be examined in more detail in Section 3.3.

It is evident that the $\alpha=2$ data behave quite differently compared to the others, see, e.g., the difference of several orders of magnitude between the Gaussian $\langle V\rangle$ curve and that for $\alpha=1.9$ in Fig. 2(b). This is due to the absence of Lévy flights steering the phase evolution. Still looking at the $\alpha=2$ case, we can again recognize two distinct behaviors, namely, above and below γ_L^{th}: at $\gamma_L<\gamma_L^{th}$ the phase stays bounded inside the initial well, thus making $\langle V\rangle$ very small, while at $\gamma_L>\gamma_L^{th}$ noise-triggered escapes can occur, so that the phase can leave the initial metastable state of the washboard potential, and a non-zero average voltage drop develops. Furthermore, for $\gamma_L>\gamma_L^{th}$ all curves for $\alpha>1.3$ seem to crowd around a common plateau.

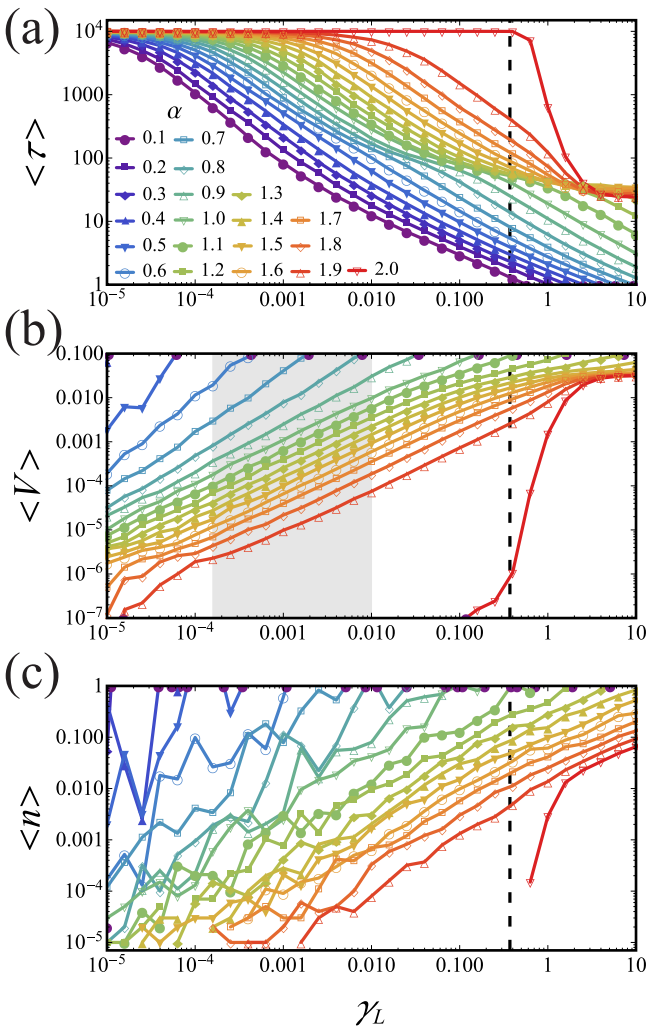

Fig. 2. *Case (a), spatially distributed noise sources.* (a) MST, $\langle\tau\rangle$, (b) average voltage drop, $\langle V\rangle$, and (c) average soliton density, $\langle n\rangle$, as a function of the Lévy noise intensity, at different value of α ranging from $\alpha=0.1$ (purple curve) to $\alpha=2$ (red curve). In panel (b), a gray shading indicates the region of noise intensity, within which the voltage increases linearly, used to compute the responsivity. Other parameters: $i_b=0.2$, $L=20$, $\beta_c=1$, $t_{\max}=10^4$, and $N_{\exp}=5\times10^3$. The lines are guides for the eye. The legend in panel (a) refers to all panels. (For interpretation of the references to color in this figure legend, the reader is referred to the web version of this article.)

Finally, we note that the behavior of the average voltage is tightly intertwined with the density of noise-induced kinks; indeed, it is evident from Fig. 2(c) that the $\langle n\rangle$ curves behave similarly to the $\langle V\rangle$ ones, *i.e.*, they appear arranged in well-spaced parallel lines with positive slope [73].

Overall, we have found in this subsection that the escape time diagnostics represents an effective tool for identifying the main parameters of a distributed Lévy source applied to an LJJ.

3.2. Case (b): homogeneous noise source

In Fig. 3 we show how $\langle\tau\rangle$ and $\langle V\rangle$ depend on γ_L, considering $\alpha\in[0.1-2]$, when the junction is affected by noisy fluctuations homogeneous across its length, *i.e.*, the case (b) in Fig. 1.

Unlike the previous case of independent noise sources, the $\langle\tau\rangle$ *versus* γ_L curves cluster in a narrower bundle, see Fig. 3(a). Interestingly, as α varies, three different regimes of noise intensities emerge: it is evident, for instance, that the MSTs for $\alpha=2$ (red curve) are significantly lower than the others for intermediate noise intensities, i.e., $\gamma_L\in(0.02-0.4)$.

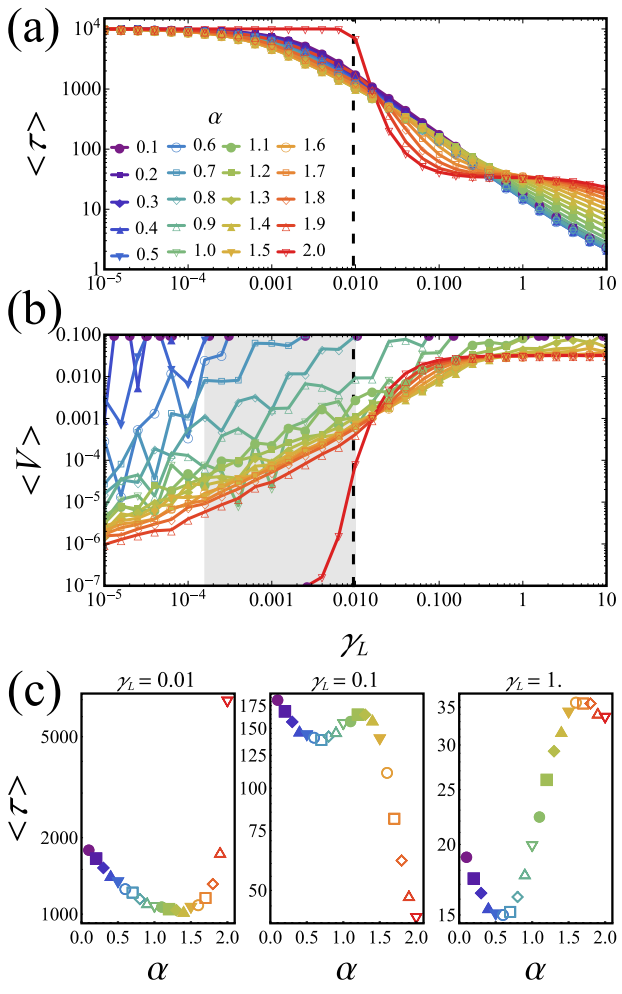

Fig. 3. *Case (b), homogeneous noise sources.* (a) MST, $\langle\tau\rangle$, and (b) average voltage drop, $\langle V\rangle$, *versus* Lévy noise intensity, at different value of α ranging from $\alpha = 0.1$ (purple curve) to $\alpha = 2$ (red curve). (c) MST *versus* α at three different noise intensities $\gamma_L = \{0.01, 0.1, 1\}$. In panel (b), a gray shading indicates the region of noise intensity, within which the voltage increases linearly, used to compute the responsivity. Other parameters: $i_b = 0.2$, $L = 20$, $\beta_c = 1$, $t_{\max} = 10^4$, and $N_{\exp} = 10^4$. The lines are guides for the eye. The legend in panel (a) refers to all panels. (For interpretation of the references to color in this figure legend, the reader is referred to the web version of this article.)

To clearly highlight the system response in these regimes, we look at MST *versus* α for $\gamma_L = \{0.01, 0.1, 1\}$, see Fig. 3(c). In all these cases we notice non-monotonic dependence of $\langle\tau\rangle$ *versus* γ_L, but with different values of α in correspondence of local minima and maxima, caused by faster and slower barrier crossing processes, respectively. In particular, at low noise intensities ($\gamma_L = 0.01$), where the tails of the Lévy noise distribution play a relevant role in the barrier crossing process [72], we observe higher $\langle\tau\rangle$, with a pronounced minimum, with respect to the values obtained in the intermediate ($\gamma_L = 0.1$) and high ($\gamma_L = 1.0$) noise intensity regimes. In other words, the index α can be used as a control parameter to make the average lifetime of the superconducting metastable state longer or shorter.

If we focus again on the MST curve for $\alpha = 2$, we observe that it reaches a plateau at $\langle\tau\rangle \equiv t_{\max}$ for noise intensities below a certain threshold, whose value is however much smaller than that in Fig. 2(a). This behavior can be explained by observing that in the present scenario, since no noise-induced kinks are expected, the activation energy in practice is given by the washboard potential energy barrier, possibly tilted by the bias current. Accordingly, Kramers rate, Eq. (14), can be

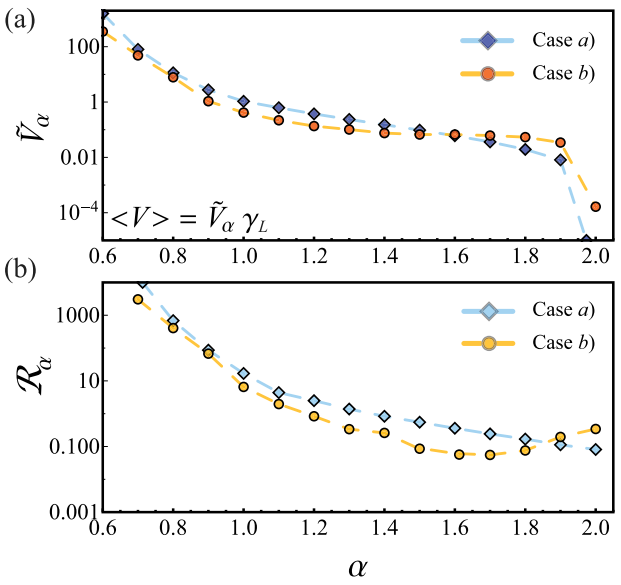

Fig. 4. (a) Fitting parameter $\widetilde{V}_\alpha$ and (b) responsivity $\mathcal{R}_\alpha = \left|\Delta\widetilde{V}_\alpha/\Delta\alpha\right|$ as a function of α for: many noise sources distributed along the junction [case (a), diamonds, $\widetilde{V}_\alpha^{(a)}$]; a homogeneous noise source affecting the whole junction [case (b), circles, $\widetilde{V}_\alpha^{(b)}$]. The parameter $\widetilde{V}_\alpha$ is obtained by fitting the $\langle V\rangle$ curves shown in the gray shaded region in Figs. 2 and 3 with the function $\widetilde{V}_\alpha \times \gamma_L$. The lines are guides for the eye. (For interpretation of the references to color in this figure legend, the reader is referred to the web version of this article.)

recast as

$$\Gamma_{(b)}(i_b, \gamma) = \frac{\omega_c}{2\pi}\left(1 - i_b^2\right)^{\frac{1}{4}} e^{-\frac{\Delta\mathcal{U}(i_b)}{L\gamma}}. \tag{15}$$

Thus, the matching of the condition $t_{\max} = \Gamma_{(b)}^{-1}(i_b, \gamma_L^{th}/\sqrt{2})$ requires $\gamma_L^{th} \sim 0.01$, *i.e.*, the black dashed line in Fig. 3(a,b).

What we have observed for the MST is also reflected in the behavior of the after-switching phase velocity. Indeed, the $\langle V\rangle$ *versus* γ_L curves still appear organized in parallel lines, which then tend to group around a common plateau at high noise intensities, see Fig. 3(b). We can still recognize a region of γ_L values in which these curves grow linearly, in a log–log plot, but the spacing between them is much smaller than in the previous case. As we will see in the next section, the difference between the two cases discussed so far can be further highlighted by looking at numerical fits and an *ad-hoc* figure of merit.

3.3. Responsivity

In Figs. 2(b) and 3(b) we shade in gray the region of noise intensities within which the voltage increases linearly; in other words, in correspondence of these γ_L values, the voltage shows a power-law trend, evidenced by well-distinct parallel lines in a log–log scale. This is in line with the power-law behavior of the MST in the presence of Lévy noise, $\langle\tau_\alpha\rangle = C(\alpha)/\gamma_L^{\mu_\alpha}$ with $\mu_\alpha \simeq 1$, discussed in Ref. [72]. It has been also shown that the average particle velocity in the presence of Lévy noise, and thus the average voltage drop, is proportional to the inverse of the MST, i.e., $\langle V\rangle \propto 1/\langle\tau_\alpha\rangle$ [29]. Thus, the $\langle V\rangle$ *versus* γ_L curves in Figs. 2(b) and 3(b) can be fitted with a function $\langle\widetilde{V}\rangle = \widetilde{V}_\alpha \times \gamma_L$, where $\widetilde{V}_\alpha$ is the fitting parameter.

Fig. 4(a) shows the behavior of the fitting parameters, $\widetilde{V}_\alpha^{(a)}$ and $\widetilde{V}_\alpha^{(b)}$, as a function of α, calculated respectively from Figs. 2(b) and 3(b) in the range of noise intensities $\gamma_L \in (10^{-4}, 10^{-2})$. For both spatially distributed and homogeneous noise sources, the fitting parameters, $\widetilde{V}_\alpha^{(a)}$ and $\widetilde{V}_\alpha^{(b)}$, respectively, tend to decrease with α. Furthermore, it can be seen that for $\alpha < 1.5$ ($\alpha > 1.5$) we find $\widetilde{V}_\alpha^{(b)} < \widetilde{V}_\alpha^{(a)}$ ($\widetilde{V}_\alpha^{(b)} > \widetilde{V}_\alpha^{(a)}$), and also that the slope of the curve $\widetilde{V}_\alpha^{(b)}$ is less than that of $\widetilde{V}_\alpha^{(a)}$. This aspect can

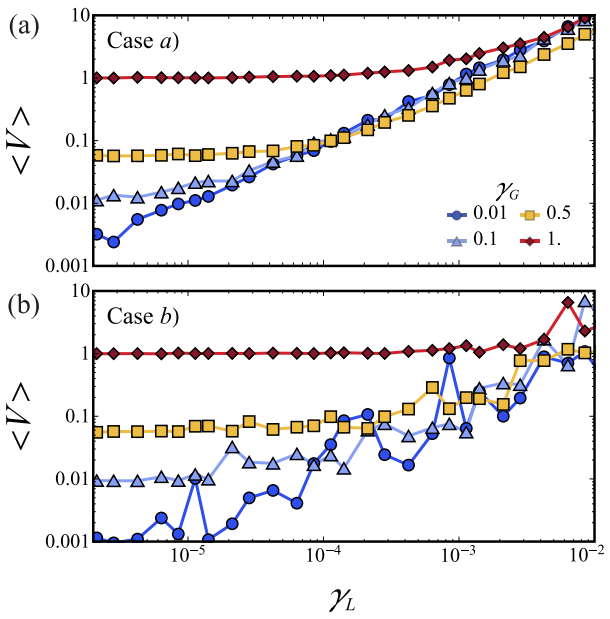

Fig. 5. Normalized average voltage drop as a function of the amplitude γ_L of the Lévy noise source, at $\alpha = 1$ and $i_b = 0.2$, for: many noise sources distributed along the junction [case (a)]; a homogeneous noise source affecting the whole junction [case (b)], in the presence of a Gaussian noise source with amplitudes $\gamma_G = \{0.01, 0.1, 0.5, 1\}$. The lines in the figure are guides for the eye. (For interpretation of the references to color in this figure legend, the reader is referred to the web version of this article.)

be quantified by the *voltage responsivity*, $\mathcal{R}_\alpha = \left|\frac{\Delta \widetilde{V}_\alpha}{\Delta \alpha}\right|$. The "sensitivity" to the Lévy component, which is more pronounced at smaller α, increases with higher responsivity, as indicated by the average voltage drop. In Fig. 4(b) we illustrate the dependence of $\mathcal{R}_\alpha$ on the stability index α, for the two noise-source configurations discussed so far. It is clear that the responsivity tends to decrease with α in both cases, but it is larger considering many distributed noise sources (except for $\alpha \lesssim 2$), as expected from the data of the MST *versus* γ_L.

3.4. Thermal noise effect

In this section, we assume that the whole system is also embedded in a thermal-noise background. We expect that a Gaussian noise source with a non-negligible amplitude, i.e., $\gamma_G \neq 0$ in Eq. (3), entails deviations from the previously described linear behavior of the voltage as a function of the Lévy noise intensity. To understand in which regimes the deviation occurs, it is sufficient to look at the voltage drop across the device.

The $\langle V \rangle$ vs. γ_L curves shown in panels (a) and (b) of Fig. 5 are obtained in the cases (a) and (b), respectively, at a fixed Lévy noise index $\alpha = 1$ and a bias current $i_b = 0.2$, considering different Gaussian noise intensities γ_G. In accordance with what has been already shown, it is evident that the curves in the case (b) appear more scattered. For $\gamma_G \lesssim 0.01$, thermal noise has, in both cases, no effects on $\langle V \rangle$, which follows a linear behavior within the entire range of γ_L values explored. For $\gamma_G > 0.01$, at low γ_L values we observe a $\langle V \rangle$ plateau, whose value increases with γ_G. This plateau corresponds to a phase dynamics dominated by Gaussian fluctuations. Comparing the panels in Fig. 5, it is evident that the value reached in the plateau is little affected by the type of Lévy noise distribution. However, the γ_L threshold above which the Lévy-ruled regime is established depends on the Lévy noise distribution. In particular, in the case (b) for Lévy noise to play a role we need a larger γ_L than in the case (a).

4. Conclusions

We have studied how stochastic Lévy-type fluctuations impact on the switching dynamics of an LJJ. In particular, we have looked at the behavior of the average lifetime of the superconducting state, $\langle \tau \rangle$, and the average voltage drop across the device, $\langle V \rangle$, as the noise intensity changes, at different values of the Lévy index α. The superconducting lifetime is obtained as the mean switching time from the initial metastable state, *i.e.*, a minimum of the tilted washboard potential, and is calculated as a nonlinear relaxation time. We have illustrated the different evolutions of the system in two distinct cases, *i.e.*, when the device is excited by: (a) a noise current consisting of many independent sources distributed along the junction length or (b) a homogeneous noise current.

Varying the Lévy noise intensity, both $\langle \tau \rangle$ and $\langle V \rangle$ exhibit a peculiar behavior, which differs significantly from the Gaussian noise case due to the occurrence of Lévy flights. In particular, we observe well-separated curves (one curve for each value of the Lévy index α) in the case of a spatially-distributed noise, while they are more closely packed in the case of a homogeneous noise source.

Moreover, in the homogeneous noise source case, the behavior of $\langle \tau \rangle$ *versus* α, at fixed noise intensities, shows peculiar non-monotonic trends, which depend on the γ_L value. The occurrence of these non-monotonicities could be attributed to the impossibility for the homogeneous noise to induce localized excitations, *i.e.*, kinks, along the junction. The analysis of the probability distribution functions of the switching times could, in principle, give further insights to elucidate the occurrence of non-monotonicities in the MST. Moreover, it might also be interesting to systematically explore the effect of the junction length on the phenomena illustrated here. We defer these additional analyses to a future work.

We have also shown that $\langle V \rangle$ grows linearly, in a log–log scale, with the Lévy noise intensity, with a slope that depends on the Lévy index α. In other words, it would in principle be possible to identify this intrinsic characteristic of the noise source through a voltage-drop analysis. For this application, we have conveniently defined the responsivity of such a "detector", and we have also discussed which of the two noise distributions, *i.e.*, spatially distributed or uniform noise source, is more advantageous. Finally, we have discussed in which regimes thermal noise may not influence or mask the effect of Lévy noise.

Our findings are particularly important to grasp the role of a non-Gaussian noise affecting the out-of-equilibrium dynamics of an LJJ. This point is relevant not only in the general framework of the nonequilibrium statistical mechanics, but also to improve the performances of this device if used as noise detector. In fact, we have proven that, even in the case of an LJJ, the study of the statistics of switching times and voltage drop can supply information on the non-Gaussian background noise, but with an extra degree of freedom compared to short JJs [29], thanks to spatially distributed excitations, *i.e.*, kinks.

Another context where the presence of Lévy noise could contribute to unveil interesting effects is the noise-controlled generation of breathers [74–77]. In particular, it has been recently predicted that noise-induced generation and long-term maintenance of breathers can be achieved by the interplay of a noise source and an oscillating force [78–80]: therefore, Lévy flights could be in principle used to trigger breathers in LJJs.

CRediT authorship contribution statement

Claudio Guarcello: Writing – review & editing, Writing – original draft, Visualization, Validation, Software, Methodology, Investigation, Formal analysis, Data curation, Conceptualization. **Giovanni Filatrella:** Writing – review & editing, Visualization, Validation, Supervision, Methodology, Investigation, Formal analysis, Conceptualization. **Duilio De Santis:** Writing – review & editing, Visualization, Validation, Methodology, Formal analysis. **Bernardo Spagnolo:** Writing – review & editing, Visualization, Validation, Supervision, Conceptualization. **Davide Valenti:** Writing – review & editing, Visualization, Validation, Supervision, Resources, Conceptualization.

Declaration of competing interest

The authors declare that they have no known competing financial interests or personal relationships that could have appeared to influence the work reported in this paper.

Data availability

Data will be made available on request.

Acknowledgments

The authors acknowledge the support of the Italian Ministry of University and Research (MUR). G.F. acknowledges the support of the PRIN 2022 PNRR Project QUESTIONs (Grant No. P2022KWFBH).

References

[1] Malomed BA. Low Temp Phys 2022;48:856.
[2] Lomdahl P, Soerensen O, Christiansen PL. Phys Rev B 1982;25:5737.
[3] McLaughlin DW, Scott AC. Phys Rev A 1978;18:1652.
[4] Parmentier RD. Solitons and long Josephson junctions. In: Weinstock H, Ralston RW, editors. The new superconducting electronics. Netherlands, Dordrecht: Springer; 1993, p. 221–48.
[5] Ustinov A. Physica D 1998;123:315.
[6] Cuevas-Maraver J, Kevrekidis P, Williams F. The sine-Gordon model and its applications: from pendula and Josephson junctions to gravity and high-energy physics. Nonlinear systems and complexity, New York: Springer; 2014.
[7] Barone A, Paterno G. Physics and applications of the Josephson effect. Wiley; 1982.
[8] Laub A, Doderer T, Lachenmann SG, Huebener RP, Oboznov VA. Phys Rev Lett 1995;75:1372.
[9] Valenti D, Denaro G, La Cognata A, Spagnolo B, Bonanno A, Basilone G, Mazzola S, Zgozi S, Aronica S. Acta Phys Pol B 2012;43:1227.
[10] Valenti D, Denaro G, Spagnolo B, Mazzola S, Basilone G, Conversano F, Brunet C, Bonanno A. Ecol Complex 2016;27:84.
[11] Valenti D, Fazio G, Spagnolo B. Phys Rev E 2018;97:062307.
[12] (Kidiyarova-Shevchenko) AH, Fedorov A, Shnirman A, Il'ichev E, Schön G. Supercond Sci Technol 2007;20:S450.
[13] Likharev KK. Physica 2012;482C:6.
[14] Monaco R, Granata C, Russo R, Vettoliere A. Supercond Sci Technol 2013;26:125005.
[15] Granata C, Vettoliere A, Monaco R. Supercond Sci Technol 2014;27:095003.
[16] Soloviev II, Klenov NV, Bakurskiy SV, Pankratov AL, Kuzmin LS. Appl Phys Lett 2014;105:202602.
[17] Guarcello C, Solinas P, Braggio A, Giazotto F. Phys Rev Appl 2018;9:034014.
[18] Guarcello C, Solinas P, Braggio A, Giazotto F. Sci Rep 2018;8:12287.
[19] Braginski AI. J Supercond Nov Magn 2019;32:23.
[20] Guarcello C, Pagano S, Filatrella G. Appl Phys Lett 2024;124:162601.
[21] Castellano MG, Torrioli G, Cosmelli C, Costantini A, Chiarello F, Carelli P, Rotoli G, Cirillo M, Kautz RL. Phys Rev B 1996;54:15417.
[22] Kim JH, Dhungana RP, Park K-S. Phys Rev B 2006;73:214506.
[23] Fedorov K, Pankratov A. Phys Rev B 2007;76:024504.
[24] Augello G, Valenti D, Pankratov AL, Spagnolo B. Eur Phys J B 2009;70:145.
[25] Fedorov KG, Pankratov AL. Phys Rev Lett 2009;103:260601.
[26] Pankratov AL, Gordeeva AV, Kuzmin LS. Phys Rev Lett 2012;109:087003.
[27] Guarcello C, Valenti D, Augello G, Spagnolo B. Acta Phys Pol B 2013;44:997.
[28] Guarcello C, Valenti D, Spagnolo B, Pierro V, Filatrella G. Phys Rev Appl 2019;11:044078.
[29] Guarcello C, Filatrella G, Spagnolo B, Pierro V, Valenti D. Phys Rev Res 2020;2:043332.
[30] Guarcello C. Chaos Solitons Fractals 2021;153:111531.
[31] Josephson B. Phys Lett 1962;1:251.
[32] Josephson BD. Rev Modern Phys 1974;46:251.
[33] Grabert H, Weiss U. Phys Rev Lett 1984;53:1787.
[34] Likharev K. Dynamics of Josephson junctions and circuits. 1986.
[35] Goldobin E. Microwave superconductivity. Springer; 2001, p. 581–614.
[36] Chechkin A, Gonchar V. Phys A 2000;277:312.
[37] Leadbeater M, Falko VI, Lambert CJ. Phys Rev Lett 1998;81:1274.
[38] Novikov DS, Drndic M, Levitov LS, Kastner MA, Jarosz MV, Bawendi MG. Phys Rev B 2005;72:075309.
[39] Chechkin AV, Gonchar VY, Klafter J, Metzler R. Fractals, diffusion, and relaxation in disordered complex systems: advances in chemical physics. 2006, p. 439, Part B.
[40] Ankerhold J. Phys Rev Lett 2007;98:036601.
[41] Leptos KC, Guasto JS, Gollub JP, Pesci AI, Goldstein RE. Phys Rev Lett 2009;103:198103.
[42] Krishnamurthy S, Ghosh S, Chatterji D, Ganapathy R, Sood AK. Nat Phys 2016;12:1134.
[43] Serdukova L, Zheng Y, Duan J, Kurths J. Chaos 2016;26:073117.
[44] Kurihara T, Aridome M, Ayade H, Zaid I, Mizuno D. Phys Rev E 2017;95:030601.
[45] Albers T, Radons G. Phys Rev Lett 2018;120:104501.
[46] Sung Y, Beaudoin F, Norris LM, Yan F, Kim DK, Qiu JY, von Lüpke U, Yoder JL, Orlando TP, Gustavsson S, Viola L, Oliver WD. Nature Commun 2019;10:3715.
[47] Bothe M, Sagues F, Sokolov IM. Phys Rev E 2019;100:012117.
[48] Vezzani A, Barkai E, Burioni R. Sci Rep 2020;10:2732.
[49] Kanazawa K, Sano TG, Cairoli A, Baule A. Nature 2020;579:364.
[50] Ariga T, Tateishi K, Tomishige M, Mizuno D. Phys Rev Lett 2021;127:178101.
[51] Lucarini V, Serdukova L, Margazoglou G. Nonlinear Process Geophys 2022;29:183.
[52] Barbosa ALR, Lima JRF, Pereira LFC. Phys Rev E 2022;106:054127.
[53] Baule A, Sollich P. Sci Rep 2023;13:3853.
[54] Jiao C, Gottwald GA. Proc R Soc A: Math Phys Eng Sci 2023;479:20230349.
[55] Briskot U, Dmitriev IA, Mirlin AD. Phys Rev B 2014;89:075414.
[56] Gattenlöhner S, Gornyi IV, Ostrovsky PM, Trauzettel B, Mirlin AD, Titov M. Phys Rev Lett 2016;117:046603.
[57] Kiselev EI, Schmalian J. Phys Rev Lett 2019;123:195302.
[58] Fonseca DB, Pereira LFC, Barbosa ALR. Phys Rev B 2023;107:155432.
[59] Fonseca DB, Barbosa ALR, Pereira LFC. Phys Rev B 2024;110:075421.
[60] Weron R. Statist Probab Lett 1996;28:165.
[61] Weron R. Correction to: On the Chambers–Mallows–Stuck Method for Simulating Skewed Stable Random Variables. University Library of Munich, Germany; 2010, RePEc:pra:mprapa:20761.
[62] Chambers JM, Mallows CL, Stuck B. J Amer Statist Assoc 1976;71:340.
[63] Binder K. Phys Rev B 1973;8:3423.
[64] Agudov NV, Malakhov AN. Radiophys Quantum Electron 1993;36:97.
[65] Malakhov A, Pankratov A. Phys C: Supercond 1996;269:46.
[66] Malakhov A, Pankratov A. Phys A 1996;229:109.
[67] Pankratov A. Phys Lett A 1997;234:329.
[68] Kuplevakhsky SV, Glukhov AM. Phys Rev B 2006;73:024513.
[69] Kramers HA. Physica 1940;7:284.
[70] The coefficient $\sqrt{2}$ stems from the different normalization of noise intensities of a Gaussian and a Lévy distribution with $\alpha = 2$.
[71] Chechkin AV, Gonchar VY, Klafter J, Metzler R. Europhys Lett 2005;72:348.
[72] Chechkin AV, Sliusarenko OY, Metzler R, Klafter J. Phys Rev E 2007;75:041101.
[73] The fluctuations that we observe in the $\langle n \rangle$ vs. γ_L curves can be smoothed out by increasing the number of experiments.
[74] Gulevich DR, Gaifullin MB, Kusmartsev FV. Eur Phys J B 2012;85:24.
[75] De Santis D, Guarcello C, Spagnolo B, Carollo A, Valenti D. Chaos Solitons Fractals 2022;158:112039.
[76] De Santis D, Guarcello C, Spagnolo B, Carollo A, Valenti D. Chaos Solitons Fractals 2023;168:113115.
[77] De Santis D, Guarcello C, Spagnolo B, Carollo A, Valenti D. Commun Nonlinear Sci Numer Simul 2022;115:106736.
[78] De Santis D, Guarcello C, Spagnolo B, Carollo A, Valenti D. Chaos Solitons Fractals 2023;170:113382.
[79] De Santis D, Guarcello C, Spagnolo B, Carollo A, Valenti D. Commun Nonlinear Sci Numer Simul 2024;131:107796.
[80] De Santis D, Spagnolo B, Carollo A, Valenti D, Guarcello C. Chaos Solitons Fractals 2024;185:115088.